

Fragile-to-strong glass transition in two-dimensional vortex liquids

I. Maccari ^{*}*Institute for Theoretical Physics, ETH Zurich, 8093 Zurich, Switzerland*L. Benfatto , C. Castellani , and J. Lorenzana *ISC-CNR and Department of Physics, Sapienza University of Rome, Piazzale A. Moro 5, 00185 Rome, Italy*C. De Michele [†]*Department of Physics, Sapienza University of Rome, Piazzale A. Moro 2, 00185 Rome, Italy*

(Received 20 September 2024; accepted 13 January 2025; published 13 February 2025)

The fragile-to-strong glass transition is a fascinating phenomenon that still presents many theoretical and experimental challenges. A major one is how to tune the fragility of a glass-forming liquid. Here, we study a two-dimensional (2D) system composed of vortices in a superconducting film, which effectively behaves as a 2D glass-forming liquid. We show that the kinetic fragility in this system can be experimentally varied by tuning a single parameter: the external magnetic field H applied perpendicularly to the film. This conclusion is supported by the direct comparison between the analysis of experimental measurements in an amorphous MoGe superconducting film and Monte Carlo simulations in a disordered XY model, that captures the universality class of the two-step melting transition. We show that by increasing disorder strength, a fragile-to-strong transition is induced, in close similarity with the experimental findings in a magnetic field. Our numerical results shed light on the evolution of the dynamical heterogeneity from a fragile-to-strong glass, as due to the subtle interplay between caging effects arising from hexatic order and strong random pinning.

DOI: [10.1103/PhysRevResearch.7.013160](https://doi.org/10.1103/PhysRevResearch.7.013160)

I. INTRODUCTION

The slowing down of the dynamics of a glass-forming liquid as it approaches the glass transition is a fascinating phenomenon that is still poorly understood. Kauzmann [1] was the first to realize that if equilibrium could be maintained during cooling, at some temperature T_K the entropy of the liquid becomes as low as that of an ordered state. However, the dynamics become so slow before T_K can be attained that equilibration is no longer possible and the system becomes a glass at a temperature $T_g > T_K$. How the dynamics slow down differs from system to system [2]. Some liquids, termed ‘strong,’ display an Arrhenius behavior, where the viscosity $\eta(T)$ is proportional to $\exp(B/T)$, which can be easily interpreted in terms of energy barriers. In contrast, other liquids, termed ‘fragile,’ exhibit a much more dramatic increase in $\eta(T)$, which is well described by the Vogel-Fulcher-Tamman (VFT) law [3–5], i.e., $\eta(T) \sim \exp[B/(T - T_0)]$. Despite being a phenomenological law, the temperature T_0 at which the viscosity diverges indicates the presence of a dynamical phase transition which is expected to coincide with the thermodynamic transition occurring at

T_K [6,7]. This extraordinary increase in viscosity has often been attributed to dynamical heterogeneity which can emerge as a result of particle-particle interactions. In colloids, the observed fragility variation [8–10] has been microscopically related to the particle potential softness [11–17] and particle deformation [18]. In two-dimensional (2D) systems, dynamical heterogeneity can also originate from the two-step melting transition from the solid to the liquid phase, as predicted by the Berezinskii-Kosterlitz-Thouless-Halperin-Nelson-Young (BKTHNY) theory [19–24]. This is indeed associated with increased hexatic correlations in the intermediate liquid phase, which lacks long-range translational order but retains orientational correlations [25–31]. Along with colloids, type-II superconducting (SC) films offer a promising platform to study the fragility of two-dimensional glass-forming liquids and shed light on its microscopic origin. When a magnetic field H is applied perpendicularly to the SC film, and it exceeds a critical threshold called H_{c1} , it starts to penetrate in the form of quantized superconducting vortices which behave as interacting classical particles, see Fig. 1(a). Each vortex carries a quantum flux $\Phi_0 = h/2e$, where h is Planck’s constant and e is the electric charge; the magnitude of the applied field thus determines the vortex density induced in the system, with $n_v = H/\Phi_0$. These vortices effectively behave as 2D Coulomb charges whose free energy landscape is ultimately determined by the interplay between their interaction potential, whose coupling constant is set by the superfluid density n_s , and the quenched disorder, which may arise from atomic-scale point defects and acts as a pinning force. At low temperatures and weak disorder, a vortex solid

^{*}Contact author: imaccari@phys.ethz.ch[†]Contact author: cristiano.demichele@uniroma1.it

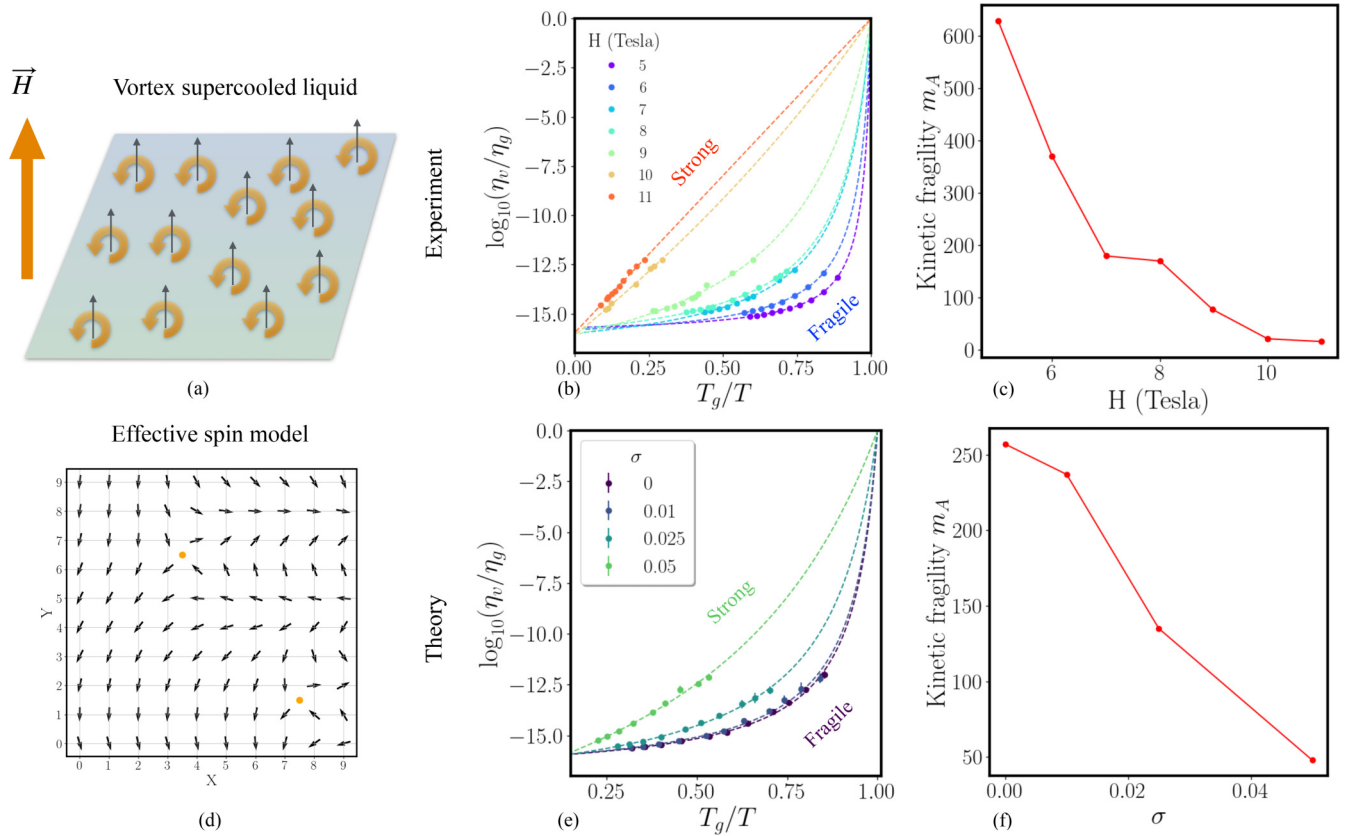


FIG. 1. (a) Schematic representation of vortex supercooled liquid forming in a SC thin film. The black arrows indicate the magnetic flux entered into the system, leading to the formation of vortices in the gauge-invariant SC phase, indicated as orange circular arrows. (b) Angell's plot for the viscosity of the 2D vortex lattice forming in an amorphous MoGe thin film. The vortex viscosity is obtained from the low-temperature resistivity $\rho(T) = \Phi_0 H / \eta_v(T)$ for different values of the applied perpendicular magnetic field H (T). The experimental data for the resistivity are those presented in [32]. As one can see, by increasing the applied field the system transitions from a fragile to a strong glass. (c) The extracted dynamic fragility of the glass-forming vortex liquid. (d) Snapshot of a portion of the spin grid numerically simulated. The vortices emerge as topological excitations of the superconducting phase and are shown here as orange dots. (e) Angell's plot for the viscosity obtained via Monte Carlo simulations on a 2D vortex lattice for different disorder strengths σ and fixed magnetic field H . By increasing σ the system transitions from a fragile to a strong glass behavior. (f) Kinetic fragility of the simulated 2D vortex liquid as a function of the quenched disorder strength σ . For both panels (b) and (e), the dashed lines correspond to a VFT fit of the data.

forms as a 2D Bragg glass [33] and the system is superconductive. The SC transition to a metallic phase coincides with the melting of the vortex solid into a vortex liquid. In a recent work [32], this framework was applied to study the melting of a weakly pinned 2D vortex lattice in amorphous MoGe SC thin films. The first vortex configurations in this compound were captured via scanning tunneling microscopy almost 20 years ago [34–36]. Yet, it was only in 2019 that the two-step melting transition, via an intermediate hexatic liquid phase, was experimentally characterized by combining transport measurements and scanning tunneling spectroscopy [37,38]. The subsequent theoretical analysis of transport data in an extended region of H and T has introduced a novel paradigm for interpreting magnetotransport measurements. That analysis relies on the fact that at low currents and temperature, the linear resistivity is directly related to the dynamics of vortices being

$$\rho(T) = (h/2e)^2 n_v \frac{D_v(T)a}{k_B T}, \quad (1)$$

with a the linear size of the vortex, $D_v(T)$ the vortex diffusion coefficient, and k_B the Boltzmann constant. By using the Stokes-Einstein relation as a working definition for the vortex viscosity $\eta_v^{-1} = \frac{D_v(T)a}{k_B T}$, Eq. (1) can be also written as $\rho(T) = (h/2e)^2 n_v / \eta_v(T)$. In Ref. [32], the linear resistivity $\rho(T)$ was analyzed in the so-called “thermally assisted flux flow” (TAFF) regime, i.e., at low currents and temperatures, where vortices overcome the energy potential barriers U via their thermal energy. In standard cases, the TAFF regime leads to an Arrhenius law for the resistivity $\rho(T) = \rho_0 \exp(-U/T)$. In Ref. [32], we reported deviations from this standard behavior. By fitting $\rho(T)$ via the VFT law, we extracted T_0 as a function of H . That allowed the identification of fragile-glass signatures in the hexatic phase and a crossover from fragile to strong glass behavior by increasing H , as signalled by the vanishing of T_0 and the restoration of an Arrhenius thermally activated motion.

Nevertheless, a theoretical model explaining the observed experimental behavior was missing, and many of the questions that this experiment raised, related to the role played

by disorder, magnetic field, and vortex interactions, remained unanswered.

Here, we provide a new theoretical analysis of the experimental data. We present Angell's plot of the experimental vortex viscosity and extract the fragility of the vortex liquid as a function of H , see Figs. 1(b) and 1(c). This result demonstrates how 2D vortex liquids forming in thin SC films offer an unprecedented opportunity to study the fragile-to-strong glass transition by varying a single parameter within the same physical system. At the same time, we propose a theoretical model able to explain the fragile-to-strong glass transition experimentally observed in terms of an effective increase of quenched disorder with H . Monte Carlo numerical simulations on a 2D XY model in the presence of a perpendicular magnetic field show how, by varying the level of quenched disorder, parametrized by σ , the vortex liquid fragility decreases similar to what is experimentally observed by varying H . The numerical results are summarized in Figs. 1(e) and 1(f). Our work presents a novel analysis of the experimental phase diagram discussed in Ref. [32] while addressing the more general question about the fate of the fragile-glass signatures of the hexatic phase by increasing the disorder strength.

This work aims at building a bridge between the soft matter community and the community working on superconductivity and strongly correlated systems.

II. EXPERIMENTAL DATA

Starting from the TAFF resistivity measured at different magnetic fields in an amorphous MoGe thin SC film [32], we extract the vortex viscosity as $\eta_v(T) = (h/2e)^2 n_v / \rho(T)$ and plot it in Fig. 1(b) according to Angell's plot prescription [39]. Conventional glass-forming liquids, at temperatures far from glass transition, typically have a viscosity η_∞ of the order of 10^{-2} Pa · s. At the glass critical temperature, when their relaxation time is of the order of 100 s, their viscosity reaches values of the order of 10^{14} Pa · s. This means that the viscosity changes by 16 orders of magnitude from the high-temperature regime to the glass critical point. According to this convention, here we define the glass transition temperature T_g as the temperature at which the viscosity becomes 16 orders of magnitude larger than the extrapolated viscosity at large temperatures, i.e., $\eta_g = 10^{16} \times \eta_v(T \rightarrow \infty) = 10^7$ Pa · s. In Fig. 1(b), different values of the applied magnetic field are shown to demonstrate the transition from a fragile to a strong vortex glass by increasing the magnetic field H . Note that in Ref. [32], the experimental resolution for the resistivity was $\rho_{\min} = 3.6 \times 10^{-4}$ mΩ/cm corresponding to $\eta_{\max} \sim 10^{-6}$ Pa · s. Although experimentally the regime of viscosity close to the conventional η_g is not accessible (i.e., $\eta_{\max} \ll \eta_g$), the difference between fragile and strong behavior clearly emerges from the data.

From the experimental values of the vortex viscosity, we then extract the value of the vortex kinetic fragility which measures the *steepness* of the temperature dependence of the liquid viscosity at the glass transition T_g [40,41]

$$m_A = \frac{d[\log(\eta_v(T)/\eta_g)]}{d[T_g/T]} \Big|_{T=T_g}. \quad (2)$$

The resulting kinetic fragility m_A as a function of the magnetic field is shown in Fig. 1(c). In real glass-forming systems, the kinetic fragility varies over one order of magnitude ranging from 17 in strong glasses like silica to 200 in fragile glasses [39]. A comparable variation is found for the kinetic fragility of a vortex-supercooled liquid by varying a single external knob H .

Note that our conclusions do not depend on the value of η_g used to define the glass. Indeed, as shown in Fig. S3 of the Supplemental Material [42], by using $\eta_g = 10^5 \eta_v(T \rightarrow \infty) = 10^{-4}$ Pa · s the Angell plot shows qualitatively the same transition from fragile to strong. On the other hand, the absolute values of the kinetic fragility depend on the choice of η_g . This is why our choice, based on the standard convention used for glassy systems, also enables a quantitative comparison between the fragility of the vortex lattice and that found in glass literature.

III. THEORETICAL MODEL

To understand the origin of the fragile-to-strong glass transition observed in 2D vortex liquids, we perform Monte Carlo (MC) numerical simulations on the 2D XY model whose Hamiltonian on a discrete lattice without disorder and at zero field reads

$$H_{XY} = -J \sum_{i,\mu=\hat{x},\hat{y}} \cos(\theta_i - \theta_{i+\mu}). \quad (3)$$

This model is the paradigmatic theoretical model for type-II superconductors that undergo a vortex-driven phase transition [43]. It describes the Josephson-like interaction between the nearest-neighbor SC islands with phase θ_i and fixed SC density $n_s \propto J$, so that vortices appear as topological excitations of the phase field, see Fig. 1(d). Studying this model for the SC phase provides us with the major gain of accessing both the superconducting response of the system and the dynamics of the vortex lattice, without the need to model an ad hoc vortex-vortex interaction.

At zero external magnetic field, the SC phase transition belongs to the Berezinskii-Kosterlitz-Thouless (BKT) universality class [19–21], where vortices and antivortices are thermally nucleated and their unbinding at the critical point destroys the superconducting order.

Here, we study a 2D XY model in the presence of a perpendicular magnetic field and quenched disorder so that Eq. (3) becomes

$$H_{XY} = - \sum_{i,\mu=\hat{x},\hat{y}} J_i^\mu \cos(\theta_i - \theta_{i+\mu} + F_i^\mu). \quad (4)$$

The SC phase of the condensate on the site i , θ_i , is minimally coupled to the external magnetic field via the Peierls substitution $F_i^\mu = \frac{2\pi}{\Phi_0} \int_{r_i}^{r_i+\mu} A_i^\mu \cdot dr_\mu$. The presence of a finite perpendicular magnetic field $H\hat{z} = \vec{\nabla} \times \vec{A}$ frustrates the ferromagnetic coupling between neighboring sites inducing in the system a finite number of vortices with a vorticity defined by the sign of $H\hat{z}$. Each vortex carries a quantum of flux Φ_0 , so that the total number of vortices in the ground state is $N_v = fL^2$, where L is the linear size of the system and the filling fraction $f = Ha^2/\Phi_0$ is given by the magnetic flux passing through a unitary plaquette of linear size $a = 1$. Differently

from the $f = 0$ case, the phase transition is now driven by the melting of the 2D vortex lattice whose nature strongly depends on the filling fraction f and quenched disorder. Similarly to a previous work [44], the presence of a quenched disorder is embedded in the Josephson couplings J_i^μ between nearest-neighboring sites i and $i + \hat{\mu}$, with $\hat{\mu} = \hat{x}, \hat{y}$. For each link $i, i + \hat{\mu}$, J_i^μ is extracted randomly from a Gaussian distribution with mean $\bar{J} = 1$ and variance σ . The disorder strength is thus controlled by σ . This choice of quenched disorder induces a vortex pinning similar to the magnetic pinning discussed in Ref. [45]. Indeed, an inhomogeneous n_s leads to a spatially inhomogeneous kinetic inductance creating regions in space where it is energetically more convenient to accommodate circulating supercurrents.

Finally, in the experiments the disorder is nominally fixed and the tuning parameter is the perpendicular magnetic field. Yet previous studies showed that increasing the magnetic field has the same effect as increasing the effect of quenched disorder. As largely discussed in Refs. [33,46–48], for moderate fields, the elastic constant associated with the vortex displacements does not significantly change with H while the quenched pinning potential behaves as $V n_v \sim VH$ where V is a characteristic vortex-pinning energy. Therefore, to avoid spurious effects due to the incommensurability between the vortex lattice and the numerical square grid [32], see Fig. 1(d), we chose to keep the total number of vortices constant while varying the level of quenched disorder. Notice that increasing the magnetic field also decreases the superfluid density. Although this effect is not explicitly included in the model, it can be described by an increase of the ratio σ/J , corresponding to an increase of the disorder strength at fixed J . Both of the above effects indicate that increasing the vortex density results in an increase of the effect of quenched disorder.

In the following, we will show how it is precisely the effective increase in quenched disorder that drives the 2D vortex liquid from a fragile to a strong glass. Note that this is very different from systems without a disordered pinning potential, such as colloids or structural glasses, where on the contrary the increase in particle density decreases the kinetic fragility of the glass [49].

IV. NUMERICAL RESULTS

The MC simulations of the model (4) are carried out on a square grid of lattice spacing $a = 1$, linear size $L = 56$, and periodic boundary conditions. We fix the external magnetic-field intensity to $f = 1/L$, resulting in $N_v = fL^2 = 56$ vortices. For each temperature and disorder level, we compute the mean value and the statistical error of a given observable by averaging both on the MC steps and on N_{samples} independent realizations of disorder. More details on the MC simulations are reported in the Supplemental Material [42].

As already mentioned, by treating vortices as topological excitations of the phase field, the model (4) allows us to study both the vortex lattice ordering and the superfluid response of the system. Furthermore, in this work, we characterize the static and dynamic properties of the vortex lattice for each level of disorder studied. This allows us to assess the fragility of the lattice as a function of the quenched disorder and

gain insights on the experimental phase diagram discussed in Ref. [32].

A. Static properties

To assess the superconducting phase transition we compute the superfluid stiffness J_s^μ , defined as the system response to a uniform twist of the gauge-invariant phase $(\theta_i - \theta_{i+\mu} + F_i^\mu) \rightarrow (\theta_i - \theta_{i+\mu} + F_i^\mu) + \Delta_\mu$ along a given direction μ

$$J_s^\mu = - \frac{1}{L^2} \frac{\partial^2 \ln Z(\Delta_\mu)}{\partial \Delta_\mu^2} \Big|_{\Delta_\mu=0}, \quad (5)$$

where $Z(\Delta_\mu)$ is the partition function of the model (4). We compute the superfluid stiffness (see Eq. S2 in the Supplemental Material [42] for its explicit expression) along both \hat{x} and \hat{y} and we label $J_s = ((J_s^x) + (J_s^y))/2$. Here and in what follows, $\langle \dots \rangle$ stays both for the thermal average over the MC steps and the $N_{\text{samples}} = 15$ independent disorder configurations (see Supplemental Material [42] for more details).

The temperature dependence of J_s is shown in Fig. 2(a) for different levels of disorder, including the clean case where $\sigma = 0$. By increasing the disorder strength, the zero temperature value of the superfluid stiffness $J_s(T = 0)$ stays almost unchanged, while the critical temperature at which $J_s \neq 0$ strongly decreases with σ . At the same time, by increasing σ the thermalization of the system becomes more challenging as reflected by the large error bars and the slightly negative values of J_s approaching the critical temperature T_c .

The vortex pinning induced by the quenched disorder competes with the vortex-vortex interaction affecting the vortex lattice order. To investigate the impact of quenched disorder on the hexatic order, we compute the six-fold orientational order parameter G_6 . To this aim, we first determine the position of the vortices from the gauge-invariant phase circulation around each unitary plaquette of the square spin grid (see Eq. (S1) in the Supplemental Material for more details [42]), and we identify the nearest neighbors of each vortex via a Delaunay triangulation of the vortex lattice. Finally, we compute the local orientational order ψ_{6j} relative to the j th vortex as

$$\psi_{6j} = \frac{1}{N_j} \sum_{k=1}^{N_j} e^{6i\theta_{jk}}, \quad (6)$$

where N_j is the number of its nearest neighbors, and θ_{jk} is the angle that the bond connecting the two neighboring vortices j and k forms with respect to a fixed direction in the plane.

The orientational order parameter G_6 is then obtained from $\Psi_6 = \frac{1}{N_v} \sum_{j=1}^{N_v} \psi_{6j}$

$$G_6 = \langle \Psi_6 \rangle, \quad (7)$$

and its corresponding susceptibility as

$$\chi_6 = \langle \Psi_6^2 \rangle - \langle \Psi_6 \rangle^2. \quad (8)$$

The temperature dependence of G_6 and χ_6 for different disorder strengths are shown in Figs. 2(b) and 2(c). At low disorder levels, the temperature where G_6 becomes finite (i.e., where the system undergoes a hexatic-to-isotropic liquid transition) weakly depends on σ , in agreement with previous results on 2D colloidal systems with random pinning [50–52].

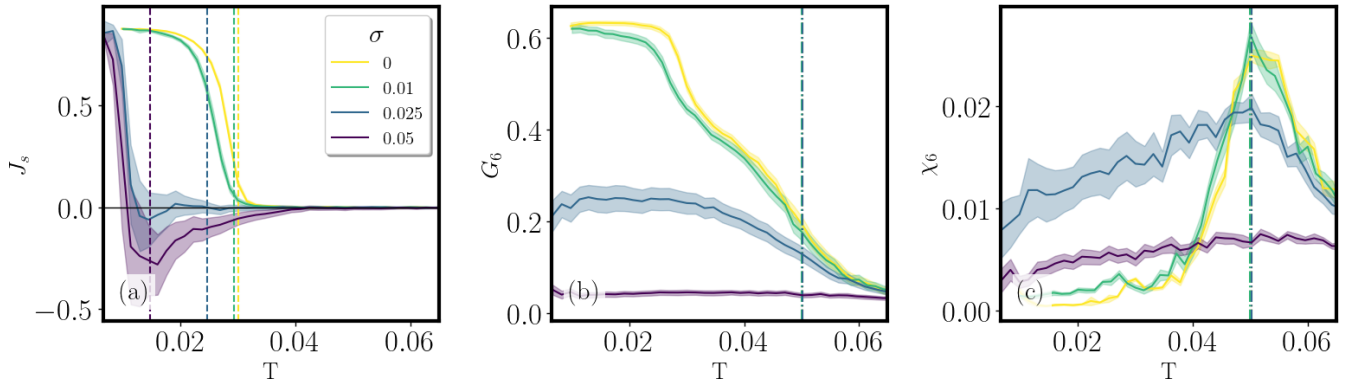


FIG. 2. Static properties of the model (4) with linear size $L = 56$ and uniform filling fraction $f = 1/L$ for different disorder strengths, as encoded in the standard deviation σ for the Gaussian distribution of the couplings. (a) Temperature dependence of the superfluid stiffness J_s . The vertical dashed lines indicate the values of T_0 extracted from the VFT fit of the vortex diffusion coefficient at each disorder level. (b), (c) Temperature dependence of the orientational order parameter G_6 and its susceptibility χ_6 . The vertical dot-dashed lines indicate $T_{\text{hex}} \simeq 0.05$, extracted for $\sigma < 0.05$ from the peak of the hexatic susceptibility. The error bars are indicated as shaded regions around the lines.

As long as the hexatic phase exists, indeed, the hexatic critical temperature, extracted from the peak in χ_6 , remains that of the clean system being $T_{\text{hex}} \simeq 0.05$, see the dot-dashed lines in Figs. 2(b) and 2(c). On the other hand, the zero-temperature value of the hexatic order parameter, i.e., $G_6(T = 0)$, strongly depends on σ , and it becomes vanishingly small at $\sigma = 0.05$, where also the hexatic susceptibility $\chi_6(T)$ does not show a clear peak. The vanishing of $G_6(T = 0)$ for a large-enough value of σ signals the destruction of the hexatic phase and the appearance of a disordered SC vortex solid.

B. Dynamical properties

To investigate further how the 2D melting transition evolves by increasing the disorder strength, we look at the dynamic properties of the system, focusing on its slowing down as it approaches the superconducting phase from the high-temperature liquid phase. We track the position of each vortex (see the Supplemental Material for more details [42]) in time and space and extract several dynamical observables for different temperatures and disorder levels.

The results for the vortex lattice dynamical autocorrelation function, and the non-Gaussian parameter, which measures the degree of dynamic heterogeneity, are discussed and shown in Figs. S1 and S2 in the Supplemental Material [42]. Here, we focus on the mean-square displacement $\langle \Delta r^2(t) \rangle$ and the vortex viscosity η_v from which we can directly characterize the vortex lattice fragility as a function of the quenched disorder. As before, $\langle \dots \rangle$ indicates the average both over the MC steps and $N_{\text{samples}} = 10$ independent realizations of disorder.

The resulting curves of $\langle \Delta r^2(t) \rangle$ for different temperatures and disorder levels are shown in Figs. 3(a)–3(d). At large temperatures, the system shows just two timescale regimes: a subdiffusive regime at short times, for distance comparable with the lattice spacing of the discrete numerical grid, and the expected diffusive regime at larger times, where $\langle \Delta r^2(t) \rangle \sim D_v t$. However, for temperatures lower than T_{hex} , indicated in Figs. 3(a)–3(d) with a grey color, a second subdiffusive regime appears, signaling the emergence of a heterogeneous dynamic. At low disorder, where a hexatic

phase exists, the heterogeneity of the vortex dynamics can be understood in terms of the quasi-long-range orientational order between vortices that prevents them from moving isotropically in the system.

That is also the case for $\sigma = 0.05$, see Fig. 3(d), where a second subdiffusive regime also emerges around $T \simeq 0.05$ despite the presence of a vanishingly small orientational order parameter, see Fig. 2(c). The non-Gaussian parameter $\alpha_2(t)$ (see Fig. S2 of the Supplemental Material [42]) also confirms the presence of heterogeneous dynamics at this disorder strength. This should be understood as a crossover regime, where a *pinning-induced* cage takes the place of the hexatic cage forming at lower disorder levels. Eventually, this will result in a transition to a strong glass behavior at increasing disorder, as will be evident from the following analysis of the vortex viscosity.

From the large-time asymptotic behavior of $\langle \Delta r^2(t) \rangle$ we extract the vortex diffusion coefficient as $D_v = \frac{1}{4} \lim_{t \rightarrow \infty} \langle \Delta r^2(t) \rangle / t$ and compute the vortex viscosity via $\eta_v = \frac{k_B T}{D_v a^2}$. Notice that the time is in units of Monte Carlo steps and, as is customary, we assume that the long-time (glassy) fictitious MC dynamics coincide with the physical dynamics upon a suitable scaling factor [53]. Because of this, dynamical quantities such as the diffusion constant or the vortex viscosity are meaningful only as relative values.

The temperature dependence of η_v , renormalized by η_g , are shown for different disorder levels in Figs. 3(e)–3(h).

At low disorder, similarly to the clean case, see Fig. 3(e), the vortex viscosity significantly deviates from the Arrhenius behavior at low temperature following instead the phenomenological VFT law

$$\eta_v = \eta_\infty \exp\left(\frac{B}{T - T_0}\right), \quad (9)$$

where $\eta_\infty = \eta(T \rightarrow \infty)$.

As the level of disorder increases, the deviation becomes less pronounced, resulting in smaller values of T_0 which eventually vanishes at even larger σ .

Note that being T_0 the temperature at which the vortex viscosity diverges, one would expect it to coincide with the

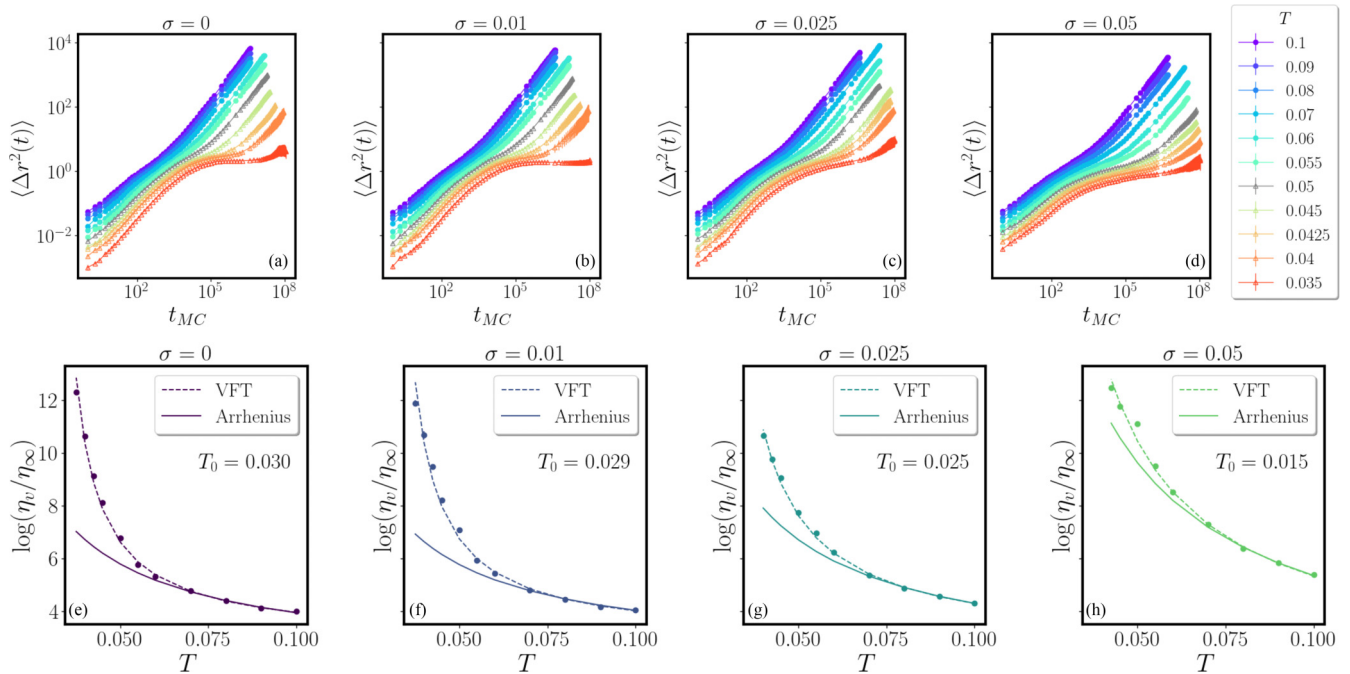


FIG. 3. Upper panels: Vortex mean-square displacement ($\Delta r^2(t)$) at different temperatures and for three different disorder levels: (a) $\sigma = 0$, i.e., clean case; (b) $\sigma = 0.01$; (c) $\sigma = 0.025$; and (d) $\sigma = 0.05$. For $\sigma < 0.05$, the grey-colored temperature indicates the critical temperature at which the hexatic liquid phase appears. For $\sigma = 0.05$, it signals the appearance of a second subdiffusive regime indicative of emerging heterogeneous dynamics despite the lack of a marked hexatic ordering as signalled by the absence of a peak in $\chi_6(T)$ for this disorder level, see Fig. 2(c). Lower panels: Temperature dependence of the natural logarithm of the vortex viscosity, $\eta_v = k_B T / D_v$, renormalized by $\eta_\infty = \eta_v(T \rightarrow \infty)$, for three different disorder levels: (e) $\sigma = 0$, i.e., clean case; (f) $\sigma = 0.01$; (g) $\sigma = 0.025$; and (h) $\sigma = 0.05$. The dashed lines in the panels (e)–(h) indicate the fit of $\eta_v(T)$ obtained using the VFT functional form, i.e., $\eta_v(T) = A \exp(\frac{B}{T-T_0})$, while the continuous lines indicate the Arrhenius fit, i.e., $\eta_v(T) = \tilde{A} \exp(\frac{B}{T})$.

temperature, T_{c,J_s} at which $J_s \neq 0$. At low disorder, $\sigma < 0.025$, we find a good agreement between T_{c,J_s} and T_0 , see Fig. 2 where T_0 are indicated as vertical dashed lines. At larger disorder, due to a significant increase of the relaxation time as reflected by larger error bars in the computed $J_s(T)$, it becomes harder to assess the coincidence between T_0 and T_{c,J_s} .

The vanishing of T_0 as a function of the quenched disorder, see Fig. 4, indicates a transition from a fragile to a strong glass behavior which appears even more evident by looking at the corresponding Angell's plot of $\log_{10}(\eta_v/\eta_g)$ versus T_g/T shown in Fig. 1(e). Here, T_g is defined as the temperature at which the viscosity reaches the threshold of $\eta_g = \eta_\infty \times 10^{16}$, with $\eta_\infty \sim 10^{-2}$ from our MC simulations. The glass temperature T_g is plotted alongside T_0 as a function of the disorder level in Fig. 4.

As already discussed, a more quantitative measure of the deviation from Arrhenius's behavior is provided by the kinetic fragility m_A , defined in Eq. (2), which is shown in Fig. 1(f). Both Angell's plot and the kinetic fragility obtained from our MC simulations are in qualitative agreement with the experimental Angell's plot and kinetic fragility shown in Figs. 1(b) and 1(c), respectively.

Hence, according to our numerical findings, the quenched disorder plays a role analogous to that of the magnetic field in the experiments, thus clarifying the nature of the fragile-to-strong glass transition experimentally observed in Ref. [32].

In the experiments, at low magnetic field H , the effect of the quenched disorder is small and a hexatic vortex liquid appears. That is characterized by a collective motion of vortices, needed to preserve orientational correlations, which results in a high kinetic fragility and a super-Arrhenius behavior.

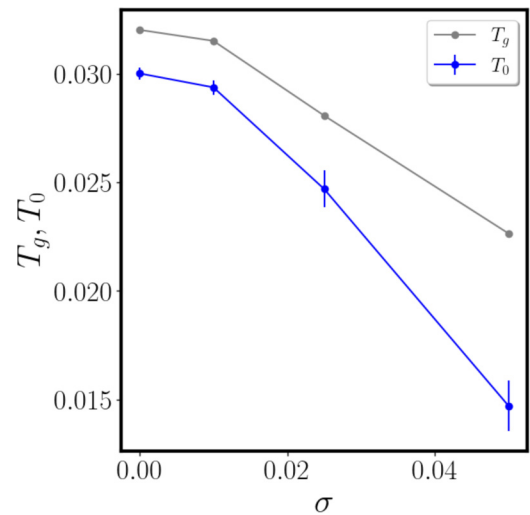


FIG. 4. Temperature T_0 , obtained from the VFT fit in Eq. (9), as a function of the disorder strength σ plotted together with the glass critical temperature T_g defined as before as $\eta_v(T_g) = \eta_\infty \times 10^{16}$.

The effective increase of quenched disorder strength with H destroys the hexatic liquid phase and the vortex motion loses its collective character as the role of random pinning becomes dominant. Eventually, the Arrhenius behavior is recovered and the vortex liquid becomes a strong glass.

V. CONCLUSION

In this work, we provided a theoretical framework to explain the fragile-to-strong glass transition occurring in an amorphous superconducting film by increasing the magnetic field H applied perpendicularly to the film. Starting from the resistivity data presented in Ref. [32], we extracted the vortex liquid viscosity and its kinetic fragility. The analysis of the experimental data, as shown in Fig. 1(b), demonstrates that tuning a single external parameter H varies the vortex liquid fragility.

To gain a deeper insight into the fragile-to-strong glass transition, we studied an effective spin model for the SC phase via Monte Carlo simulations. Since in SC thin films increasing H corresponds to increasing the effective quenched disorder, we studied the transition at fixed H by increasing the disorder strength. We showed how the level of the effective quenched disorder can determine the nature of the glass-forming liquid. Indeed, alongside a progressive destruction of the orientational order, the increase of the disorder makes the glass stronger. That can be understood in terms of disorder potential energy barriers competing with the vortex-vortex interactions. At low disorder, the glass-forming vortex liquid exhibits a hexatic liquid phase resulting in a fragile glass behavior. By increasing the disorder, the vortex liquid orientational order get progressively disrupted by random pinning until the vortex dynamic becomes the dynamic of individual vortices. That is controlled by a single timescale associated with the disorder potential so that the vortex supercooled liquid recovers an Arrhenius-like activated dynamics. Interestingly, in the high-disorder regime, we observed a logarithmic behavior in the long-time decay of the intermediate scattering function (see Fig. S1 of the Supplemental Material [42]), which reflects the competition between two distinct mechanisms slowing down the vortex relaxation, i.e., the (hexatic) caging and pinning [54].

In the present work, we used a weak Gaussian distributed quenched disorder. However, other kinds of disorder may affect the vortex dynamics in different ways. Exploring how different quenched disorders modify the observed fragile-to-strong glass transition is an interesting question that we will face in a future study.

A related question is the effect of different types of quenched disorder on the configurational entropy S_c . Indeed, quenched disorder may act by blocking out some particles, reducing the number of possible states and thus decreasing S_c [55,56] or by introducing frustration that conversely increases the configurational entropy [57]. In the first case, the Kauzmann temperature should increase with the disorder strength, while it should decrease in the second case. In our model, T_0 decreases with the increase of disorder. However, the generality of this result, and its dependence on the particular kind of disorder introduced, call for further investigations.

In conclusion, our study identifies 2D vortex lattices forming in type-II superconductors as an ideal platform to investigate the fragile-to-strong glass transition. On the one hand, they offer good control over the level of intrinsic disorder present in the sample, which can be increased by reducing the film thickness or artificially engineered, e.g., by building ordered nanopores geometries where the SC order parameter is suppressed, see Refs. [58,59] and references therein. Most importantly, the nature of the glass-forming liquid can be controlled by an external parameter, i.e., the magnetic field, enabling a systematic study of the interplay between disorder, orientational correlations, and vortex density. Beyond 2D thin superconducting films, layered three-dimensional (3D) superconductors may also provide new insights into the nature of the glass transition, including the evolution of the vortex lattice fragility through the 2D to 3D crossover.

ACKNOWLEDGMENTS

We would like to thank Dragana Popović for sharing the experimental data presented in Ref. [32] and P. Raychaudhuri for useful discussions. I.M. acknowledges financial support by the Swiss National Science Foundation (SNSF) via the SNSF postdoctoral Grant No. TMPFP2_217204. L.B. acknowledges financial support by the EU under project MORE-TEM ERC-Syn Grant Agreement No. 951215 and by Sapienza University of Rome under Projects Ateneo No. 2022 RP1221816662A977 and No. 2023 RM123188E357C540. J.L. acknowledges financial support through Projects PRIN 20207ZXT4Z QT-FLUO and CNR-CONICET 2023-2024 NMES. C.D.M. acknowledges financial support from the European Union—Next Generation EU (MUR-PRIN2022 TAMEQUAD CUP:B53D23004500006) and from ICSC—Centro Nazionale di Ricerca in High-Performance Computing, Big Data, and Quantum Computing, funded by the European Union—NextGenerationEU.

-
- [1] W. Kauzmann, The nature of the glassy state and the behavior of liquids at low temperatures, *Chem. Rev.* **43**, 219 (1948).
 - [2] C. A. Angell, Formation of glasses from liquids and biopolymers, *Science* **267**, 1924 (1995).
 - [3] H. Vogel, The temperature dependence law of the viscosity of fluids, *Phys. Z.* **22**, 645 (1921).
 - [4] G. S. Fulcher, Analysis of recent measurements of the viscosity of glasses, *J. Am. Ceram. Soc.* **8**, 339 (1925).
 - [5] G. Tammann and W. Hesse, Die abhängigkeit der viscosität von der temperatur bei unterkühlten flüssigkeiten, *Zeitschrift für anorganische und allgemeine Chemie* **156**, 245 (1926).
 - [6] A. Cavagna, Supercooled liquids for pedestrians, *Phys. Rep.* **476**, 51 (2009).
 - [7] G. Ruocco, F. Sciortino, F. Zamponi, C. De Michele, and T. Scopigno, Landscapes and fragilities, *J. Chem. Phys.* **120**, 10666 (2004).

- [8] R. P. Seekell III, P. S. Sarangapani, Z. Zhang, and Y. Zhu, Relationship between particle elasticity, glass fragility, and structural relaxation in dense microgel suspensions, *Soft Matter* **11**, 5485 (2015).
- [9] V. Nigro, R. Angelini, M. Bertoldo, F. Bruni, M. A. Ricci, and B. Ruzicka, Dynamical behavior of microgels of interpenetrated polymer networks, *Soft Matter* **13**, 5185 (2017).
- [10] V. Nigro, B. Ruzicka, B. Ruta, F. Zontone, M. Bertoldo, E. Buratti, and R. Angelini, Relaxation dynamics, softness, and fragility of microgels with interpenetrated polymer networks, *Macromolecules* **53**, 1596 (2020).
- [11] J. Mattsson, H. M. Wyss, A. Fernandez-Nieves, K. Miyazaki, Z. Hu, D. R. Reichman, and D. A. Weitz, Soft colloids make strong glasses, *Nature (London)* **462**, 83 (2009).
- [12] J. Krausser, K. H. Samwer, and A. Zaccone, Interatomic repulsion softness directly controls the fragility of supercooled metallic melts, *Proc. Natl. Acad. Sci. USA* **112**, 13762 (2015).
- [13] A. E. Lagogianni, J. Krausser, Z. Evenson, K. Samwer, and A. Zaccone, Unifying interatomic potential, $g(r)$, elasticity, viscosity, and fragility of metallic glasses: Analytical model, simulations, and experiments, *J. Stat. Mech.: Theory Exp.* (2016) 084001.
- [14] P. van der Scheer, T. van de Laar, J. van der Gucht, D. Vlassopoulos, and J. Sprakel, Fragility and strength in nanoparticle glasses, *ACS Nano* **11**, 6755 (2017).
- [15] J. Krausser, A. E. Lagogianni, K. Samwer, and A. Zaccone, Disentangling interatomic repulsion and anharmonicity in the viscosity and fragility of glasses, *Phys. Rev. B* **95**, 104203 (2017).
- [16] P. Lunkenheimer, F. Humann, A. Loidl, and K. Samwer, Universal correlations between the fragility and interparticle repulsion of glass-forming liquids, *J. Chem. Phys.* **153**, 124507 (2020).
- [17] Z. Yu, D. Morgan, M. D. Ediger, and B. Wang, Understanding the fragile-to-strong transition in silica from microscopic dynamics, *Phys. Rev. Lett.* **129**, 018003 (2022).
- [18] N. Gnan and E. Zaccarelli, The microscopic role of deformation in the dynamics of soft colloids, *Nat. Phys.* **15**, 683 (2019).
- [19] V. L. Berezinsky, Destruction of long-range order in one-dimensional and two-dimensional systems possessing a continuous symmetry group II. quantum systems, *Zh. Eksp. Teor. Fiz.* **61**, 1144 (1972) [*Sov. Phys. JETP* **34**, 610 (1972)].
- [20] J. M. Kosterlitz and D. J. Thouless, Ordering, metastability and phase transitions in two-dimensional systems, *J. Phys. C* **6**, 1181 (1973).
- [21] J. M. Kosterlitz, The critical properties of the two-dimensional xy model, *J. Phys. C* **7**, 1046 (1974).
- [22] B. I. Halperin and D. R. Nelson, Theory of two-dimensional melting, *Phys. Rev. Lett.* **41**, 121 (1978).
- [23] D. R. Nelson and B. I. Halperin, Dislocation-mediated melting in two dimensions, *Phys. Rev. B* **19**, 2457 (1979).
- [24] A. P. Young, Melting and the vector Coulomb gas in two dimensions, *Phys. Rev. B* **19**, 1855 (1979).
- [25] R. Zangi and S. A. Rice, Cooperative dynamics in two dimensions, *Phys. Rev. Lett.* **92**, 035502 (2004).
- [26] H. Shiba, A. Onuki, and T. Araki, Structural and dynamical heterogeneities in two-dimensional melting, *Europhys. Lett.* **86**, 66004 (2009).
- [27] T. Kawasaki and H. Tanaka, Structural signature of slow dynamics and dynamic heterogeneity in two-dimensional colloidal liquids: Glassy structural order, *J. Phys.: Condens. Matter* **23**, 194121 (2011).
- [28] E. P. Bernard and W. Krauth, Two-step melting in two dimensions: First-order liquid-hexatic transition, *Phys. Rev. Lett.* **107**, 155704 (2011).
- [29] S. C. Kapfer and W. Krauth, Two-dimensional melting: From liquid-hexatic coexistence to continuous transitions, *Phys. Rev. Lett.* **114**, 035702 (2015).
- [30] B. van der Meer, W. Qi, J. Sprakel, L. Filion, and M. Dijkstra, Dynamical heterogeneities and defects in two-dimensional soft colloidal crystals, *Soft Matter* **11**, 9385 (2015).
- [31] I. Tah, S. Sengupta, S. Sastry, C. Dasgupta, and S. Karmakar, Glass transition in supercooled liquids with medium-range crystalline order, *Phys. Rev. Lett.* **121**, 085703 (2018).
- [32] I. Maccari, B. K. Pokharel, J. Terzic, S. Dutta, J. Jesudasan, P. Raychaudhuri, J. Lorenzana, C. De Michele, C. Castellani, L. Benfatto, and D. Popović, Transport signatures of fragile glass dynamics in the melting of the two-dimensional vortex lattice, *Phys. Rev. B* **107**, 014509 (2023).
- [33] T. Giamarchi and P. Le Doussal, Elastic theory of flux lattices in the presence of weak disorder, *Phys. Rev. B* **52**, 1242 (1995).
- [34] G. J. C. van Baarle, A. M. Troianovski, P. H. Kes, and J. Aarts, STM imaging of vortex configurations in films of a-Mo₃Ge through a Au layer, *Physica C: Superconductivity* **369**, 335 (2002).
- [35] G. J. C. van Baarle, A. M. Troianovski, T. Nishizaki, P. H. Kes, and J. Aarts, Imaging of vortex configurations in thin films by scanning-tunneling microscopy, *Appl. Phys. Lett.* **82**, 1081 (2003).
- [36] I. Guillamón, H. Suderow, A. Fernández-Pacheco, J. Sesé, R. Córdoba, J. M. De Teresa, M. R. Ibarra, and S. Vieira, Direct observation of melting in a two-dimensional superconducting vortex lattice, *Nat. Phys.* **5**, 651 (2009).
- [37] I. Roy, S. Dutta, A. N. R. Choudhury, S. Basistha, I. Maccari, S. Mandal, J. Jesudasan, V. Bagwe, C. Castellani, L. Benfatto, and P. Raychaudhuri, Melting of the vortex lattice through intermediate hexatic fluid in an a -MoGe thin film, *Phys. Rev. Lett.* **122**, 047001 (2019).
- [38] S. Dutta, I. Roy, S. Mandal, J. Jesudasan, V. Bagwe, and P. Raychaudhuri, Extreme sensitivity of the vortex state in a -MoGe films to radio-frequency electromagnetic perturbation, *Phys. Rev. B* **100**, 214518 (2019).
- [39] C. A. Angell, Relaxation in liquids, polymers and plastic crystals—strong/fragile patterns and problems, *J. Non-Cryst. Solids*, **131-133**, 13 (1991).
- [40] D. J. Plazek and K. L. Ngai, Correlation of polymer segmental chain dynamics with temperature-dependent time-scale shifts, *Macromolecules* **24**, 1222 (1991).
- [41] R. Böhmer and C. A. Angell, Correlations of the nonexponentiality and state dependence of mechanical relaxations with bond connectivity in Ge-As-Se supercooled liquids, *Phys. Rev. B* **45**, 10091 (1992).
- [42] See Supplemental Material at <http://link.aps.org/supplemental/10.1103/PhysRevResearch.7.013160> for details on the MC numerical simulations, we explain how a vortex is detected in our numerical spin model, and we provide the full expression for the superfluid stiffness response function. Furthermore, we present the numerical results for the dynamical autocorrelation function and the non-Gaussian parameter for all the disorder levels

- investigated. Finally, we show the experimental and numerical Angell plots for a different choice of η_g .
- [43] K. Fossheim and A. Sudboe, *Superconductivity: Physics and Applications* (Wiley, New York, 2005).
- [44] I. Maccari, L. Benfatto, and C. Castellani, Uniformly frustrated XY model: Strengthening of the vortex lattice by intrinsic disorder, *Condensed Matter* **6**, 42 (2021).
- [45] A. M. Campbell and J. Evetts, *Critical Currents in Superconductors* (Taylor & Francis, London, 1972).
- [46] T. Giamarchi and P. Le Doussal, Elastic theory of pinned flux lattices, *Phys. Rev. Lett.* **72**, 1530 (1994).
- [47] T. Giamarchi and P. Le Doussal, Phase diagrams of flux lattices with disorder, *Phys. Rev. B* **55**, 6577 (1997).
- [48] T. Giamarchi and S. Bhattacharya, Vortex phases, in *High Magnetic Fields: Applications in Condensed Matter Physics and Spectroscopy*, edited by C. Berthier *et al.* (Springer, Berlin, 2002), p. 314.
- [49] I. Saika-Voivod, P. H. Poole, and F. Sciortino, Fragile-to-strong transition and polyamorphism in the energy landscape of liquid silica, *Nature (London)* **412**, 514 (2001).
- [50] S. Deuschländer, T. Horn, H. Löwen, G. Maret, and P. Keim, Two-dimensional melting under quenched disorder, *Phys. Rev. Lett.* **111**, 098301 (2013).
- [51] E. N. Tsiok, E. A. Gaiduk, Y. D. Fomin, and V. N. Ryzhov, The influence of random pinning on the melting scenario of two-dimensional soft-disk systems, *Mol. Phys.* **117**, 2910 (2019).
- [52] N. Shankaraiah, S. Sengupta, and G. I. Menon, Orientational correlations in fluids with quenched disorder, *J. Chem. Phys.* **151**, 124501 (2019).
- [53] L. Berthier and W. Kob, The Monte Carlo dynamics of a binary Lennard-Jones glass-forming mixture, *J. Phys.: Condens. Matter* **19**, 205130 (2007).
- [54] T. Sentjabrskaja, E. Zaccarelli, C. D. Michele, F. Sciortino, P. Tartaglia, T. Voigtmann, S. U. Egelhaaf, and M. Laurati, Anomalous dynamics of intruders in a crowded environment of mobile obstacles, *Nat. Commun.* **7**, 11133 (2016).
- [55] C. Cammarota and G. Biroli, Ideal glass transitions by random pinning, *Proc. Natl. Acad. Sci. USA* **109**, 8850 (2012).
- [56] I. Williams, F. Turci, J. E. Hallett, P. Crowther, C. Cammarota, G. Biroli, and C. P. Royall, Experimental determination of configurational entropy in a two-dimensional liquid under random pinning, *J. Phys.: Condens. Matter* **30**, 094003 (2018).
- [57] S. Chakrabarty, S. Karmakar, and C. Dasgupta, Dynamics of glass forming liquids with randomly pinned particles, *Sci. Rep.* **5**, 12577 (2015).
- [58] S. Bose, A review of superconductivity in nanostructures - from nanogranular films to anti-dot arrays, *Supercond. Sci. Technol.* **36**, 063003 (2023).
- [59] A. Verma, R. Vedin, J. Jesudasan, J. Lidmar, I. Maccari, and S. Bose, BKT phase transition in nanoporous films of superconducting NbN, [arXiv:2410.22704](https://arxiv.org/abs/2410.22704).